Organic Chemistry

Helically and Linearly Fused Rylenediimide-Hexabenzocoronenes

Carolin Dusold[+],[a] Philipp Haines[+],[b] Benedikt Platzer,[b] Dirk M. Guldi,*[b] and Andreas Hirsch*[a]

Abstract: Perylene- as well as naphthalenediimides were fused to hexabenzocoronenes (HBCs) at their imide position to realize highly π-extended donor–acceptor (D–A)-hybrids. Successful isomer separation in the first step was decisive to guarantee a straightforward synthetic sequence. Hexaphenylbenzenes as precursors were accessed via Diels–Alder reactions and reacted in a Scholl oxidation to yield the respective HBC derivatives. The fully conjugated benzimidazole linker, which separates the electron donating HBC from the electron accepting rylenediimide, enabled the formation of either a linear or a helical configuration. Largely different chemical, physical, and optoelectrical characteristics were noted for the two configurations. What stood out was their aggregation and their excited state deactivation depending on the solvent polarity. Results from global analysis of the femtosecond transient absorption data corroborated the formation of a charge-transfer (CT) state that is stabilized in the helically fused configuration relative to the linear analogue. However, a comparison with spectroelectrochemical experiments failed to disclose evidence for a charge-separated (CS) state.

Introduction

For the development and improvement of organic optoelectronic devices such as organic solar cells, the design of suitable conjugated (macro)molecules is crucial. Therefore, suitable systems must meet specific demands such as the possibility to photogenerate electron–hole pairs, their separation, and a high charge-carrier mobility. Moreover, the arrangement of both electron donor (D) and electron acceptor (A), leading to a high degree of order within the active layer, was found to be indispensable for a high efficiency of molecular electronics.[1] In this case, versatility of their synthesis and the flexibility regarding functionalization is important to tune their optoelectronic properties. Hexa-*peri*-hexabenzocoronene[2] (HBC) and perylenediimide[3] (PDI), both featuring interesting electronic properties as well as extended π-conjugation and π-stacking, have already been successfully utilized as excellent blends of D and A[4] with the HBC acting as D and PDI acting as A, with promising results. It was, however, found that besides such blends, the use of conjugates that contain both D and A is a great advantage.[5] Covalently linked D–A systems offer the possibility to control the self-organization, resulting in a more efficient photophysical activity and, in turn, attracted a lot of attention recently. In addition, the importance of the spacer between D and A must be taken into consideration. The nature of the spacer influences the performance of photoinduced charge separation and represents an interesting research topic.[6] Previous work on covalently linked HBC–PDI systems, including different spacer motifs, gained significant insights into their fundamental energy and electron transfer processes.[7] In our previous study, we investigated such D–A systems in terms of their photophysical activity, with the HBC connected to the rylenediimide via the imide-*N*-position without any additional linker.[8] We recently expanded the concept and merged two naphthalenediimides (NDIs) to one HBC core through a benzimidazole-bridge, generating a chiral superstructure with a diaza-[7]helicene.[9] Our current approach is to fuse only one rylenediimide to the HBC core, but enlarge the library by utilizing not only NDIs but also PDIs as the second building block. During the synthesis we generated two isomers, that is, a linear and a helical constitution as depicted in Figure 1. The linear isomer has a more planar structure, while the helical compound displays a significant conformational distortion as a result of the newly formed [5]-heterohelicene. We separated and analyzed both linearly- and helically fused derivatives to gather sound insights into how the structural nature of the

[a] C. Dusold,[+] Prof. Dr. A. Hirsch
Department of Chemistry and Pharmacy
Friedrich-Alexander-University Erlangen-Nuremberg
Nikolaus-Fiebiger-Straße 10, 91058 Erlangen (Germany)
E-mail: andreas.hirsch@fau.de

[b] P. Haines,[+] B. Platzer, Prof. Dr. D. M. Guldi
Department of Chemistry and Pharmacy
Friedrich-Alexander-University Erlangen-Nuremberg
Egerlandstrasse 3, 91058 Erlangen (Germany)
E-mail: dirk.guldi@fau.de

[+] These authors contributed equally to this work.

Supporting information and the ORCID identification number(s) for the author(s) of this article can be found under: https://doi.org/10.1002/chem.202005235.

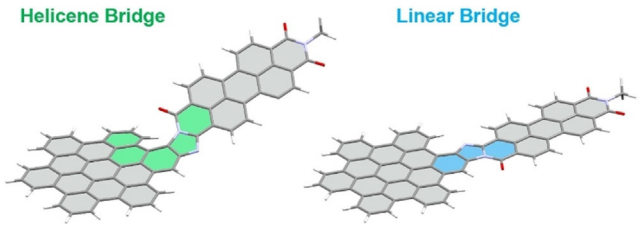

Figure 1. General structure of an HBC and a perylenediimide fused via a helical bridging unit (left) or a linear bridging unit (right).

spacer effects the properties of such D–A systems. In this contribution, we synthesized and probed a series of fully conjugated, π-extended D–A systems, having either a linear or a helical spacer.

Results and Discussion

Synthesis and characterization

The general strategy to access the desired helical and linear HBCs is illustrated in Scheme 1. We followed the common approach of Diels–Alder reactions of tetracyclone with tolanes, followed by Scholl-type oxidations.

Therefore, generation of the tolane precursors providing the precise structural conditions that lead to either helical or linear bridging is crucial.

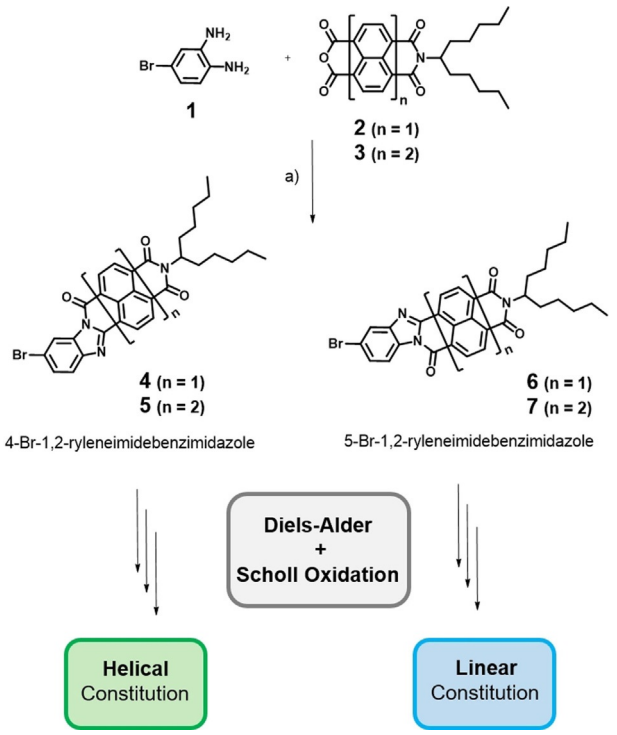

Scheme 1. Synthesis of key-compounds 4/5-Br-1,2-ryleneimidebenzimidazole isomers **4**, **5**, **6** and **7** and the subsequent general synthetic strategy based on a combination of Diels–Alder and Scholl oxidation to generate the final HBC compounds with either helical or linear constitution. (a) Imidazole, 120–160 °C, 1–3 h, yields: 36% (**4**), 24% (**5**), 42% (**6**), 29% (**7**).

The synthesis started with a condensation reaction of the naphthalene-monoimide **2**[8a] ($n=1$) as well as the perylene-monoimide **3**[8a] ($n=2$) with diamino-bromobenzene **1** (Scheme 1). Already during this reaction, two constitutional isomers are formed in each case, the 4-Br-1,2-ryleneimidebenzimidazole **4** and **5** as well as 5-Br-1,2-ryleneimidebenzimidazole **6** and **7**. For both the naphthalene- as well as the perylene-derivatives, the two isomers can easily be separated by column chromatography and were fully characterized, revealing remarkable differences regarding their NMR and optical properties (see Supporting Information S1 for details). Clear assignment of the spectra to each isomer was possible by X-ray analysis as previously reported.[9] The separation of the two isomers turned out to become the key step in this synthetic sequence. Depending on which isomer is used in the following reactions, the constitution of the product is determined. If the pure isomers 4-Br-1,2-ryleneimidebenzimidazole **4** or **5** are reacted further, the rylenediimide and the HBC subunits in **18** and **19** are connected via a helical bridging moiety. When 5-Br-1,2-ryleneimidebenzimidazole **6** or **7** are utilized as starting material, the HBC-products **20** and **21** exhibit a linear character. Furthermore, it is of great advantage since from now on, all following reactions can be performed simultaneously for each isomer in a straightforward manner without the challenge of isomer-separation during work up (Scheme 2). In a next step, palladium-catalyzed Sonogashira cross-coupling reactions of 4-*tert*-butylphenylacetylene **8**[10] with each Br-species **4**, **5**, **6** and **7** afforded the four tolane precursors **9**, **10**, **11** and **12** in a pure form in good yields. The tolanes were reacted in a Diels–Alder reaction with tetracyclone **13**–[11] at 220 °C, yielding the NDI–HPBs **14** and **16** in 58% and 79% yield as well as the PDI–HPBs **15** and **17** in 49% and 84% yield, respectively. Finally, Scholl oxidation results in the successful formation of the desired products with the NDI/PDI fused to the planar core of the HBC.

The final planarization reaction leads to the formation of a full extended, conjugated π-system with the two different spatial arrangements, depending on which Br-isomer was used in a first step. Highlighted in green in Scheme 2 is the [5]-azahelicene bridge of helical HBCs **18** and **19**. In contrast to that, the HBC-products **20** and **21** exhibit a linear character (highlighted in blue) with a complete planar structure.

The structural difference of the helical and linear isomers has a significant impact on the physical and spectroscopic properties. As a consequence of the linear, planar constitution, intermolecular aggregation, in particular strong π–π interaction of the aromatic surface, is favored. This leads to a decreased solubility and thus to characterization problems. Especially in case of the linear HBC–NDI **20** we could only obtain a satisfactory ^{1}H NMR spectrum using [D_8]toluene at high temperature of 100 °C (Figure S24). However, the structure of **20** was confirmed by APPI HRMS (atmospheric pressure photoionization high-resolution mass spectrometry), featuring a mass peak at 1218.6503 *m/z*. For the linear PDI analogue HBC–PDI **21**, the bulky *tert*-butyl-phenoxy substituents on the PDI bay-position hinder aggregation and therefore enable complete characterization. In contrast, the helical compounds **18** and **19** display a significant conformational distortion due to the [5]-azahelicene

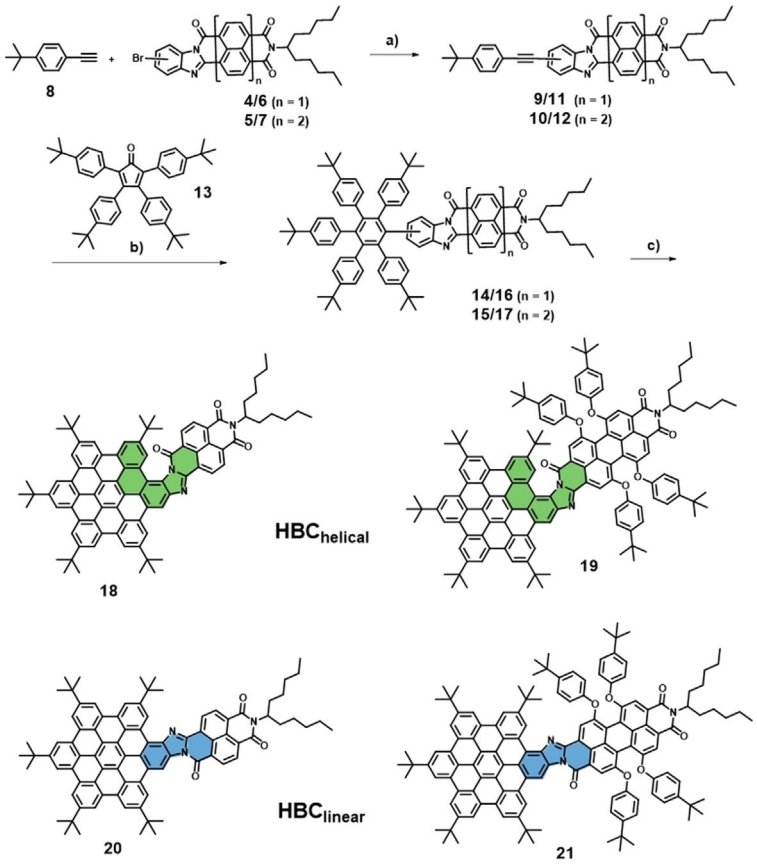

Scheme 2. Synthesis of helical HBCs **18** and **19** as well as linear HBCs **20** and **21**. (a) $PdCl_2(PPh_3)_2$, CuI, Et_3N, toluene, 80 °C, over-night, yields: 60% (**9**), 100% (**10**), 76% (**11**), 92% (**12**); (b) tetracyclone **13**, toluene, 220 °C, 24 h, yields: 58% (**14**), 49% (**15**), 79% (**16**), 84% (**17**); (c) $FeCl_3$, CH_3NO_2, DCM, 0 °C, overnight, yields: 88% (**18**), 95% (**19**), 85% (**20**), 85% (**21**).

subunit, leading to a nonplanar structure. Hence, PDI- as well as NDI-derivatives exhibit good solubility in common organic solvents and were fully characterized.

The successful performance of the Scholl oxidation was confirmed by proton NMR spectroscopy. In general, the resonances of the HPB-moiety between 6.60–6.90 ppm disappeared completely while simultaneously, new downfield shifted signals emerge that can be assigned to the HBC-protons (see Supporting Information S3). The structural difference between linear and helical isomers is also reflected in the NMR spectra as demonstrated for perylene-HBCs **19** and **21** in Figure 2. Assignment was possible with the help of correlated spectroscopy (COSY) and nuclear Overhauser effect (NOE) measurements (see Supporting Information S2).

Whereas resonance of the perylene-Hs and major of the HBC-Hs appear in similar regions, hydrogen atoms at the HBC next to the bridging units, highlighted in red and orange, show remarkable differences. The signal of the proton "within" the [5]-azahelicene subunit in compound **19** (Figure 2, top, red) is high-field shifted to 8.46 ppm relative to the remaining HBC-protons between 9.20–9.75 ppm. In the linear isomer **21**, with the "shielding effect" of the helicene missing, hydrogen atom highlighted in red is strongly downfield shifted to 11.60 ppm. The resonances at 9.75 ppm (**19**) and 10.44 ppm (**21**) show no COSY-correlation and therefore can be assigned to the protons at the HBC rim highlighted in orange. Similar features were found for the helical HBC–NDI **18** (see Supporting Information S2); however, the resolution of the spectra of linear HBC–NDI **20** was too poor for performing further NMR-experiments.

The conversion of the HPBs to the corresponding HBCs can be monitored by UV/Vis absorption and fluorescence measurements of the PDI–HPB precursors **15** and **17**, on the one hand, and the PDI–HBC products **19** and **21**, on the other hand (Figure S48A). Compounds **15** and **17** feature the characteristic perylene fine structure between 400–650 nm, with the absorption maximum of **15** being slightly redshifted (616 nm) compared to **17** (610 nm). After planarization, the products **19** and **21** exhibit a new intensive absorption between 330–420 nm, which is assigned to the newly formed HBC. The perylene-absorptions are subject to a red-shifting, broadening and decrease in intensity. In addition, the bright, pink fluorescence emission of both HPB precursors is quenched after Scholl oxidation upon excitation of the perylene as well as the HBC band, indicating an electronic communication between the two chromophores. The NDI-analogues present similar characteristics (Figure S48B). The broad naphthalene absorption of NDI-HPBs **14** (483 nm) and **16** (435 nm) experiences a significant redshift, while at the same time, the strong HBC-bands re-emerged. In the following, more detailed absorption- and emission-studies on linearly- and helically fused HBCs are presented.

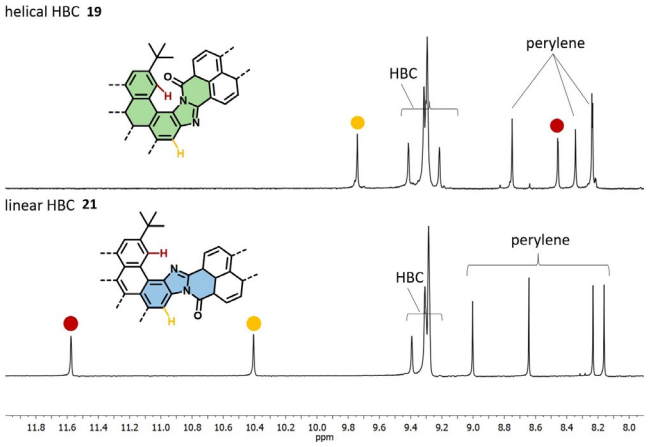

Figure 2. Aromatic region of ^1H NMR spectra of helical PDI–HBC **19** (top) and linear PDI–HBC **21** (bottom).

Absorption properties

Steady-state absorption spectra were recorded in toluene and benzonitrile PhCN. Helical PDI-HBC **19** exhibits in toluene the widely known HBC-related absorption features, namely the β-, p-, and α-bands at 371, 400, 440, and 466 nm, next to the S_1-

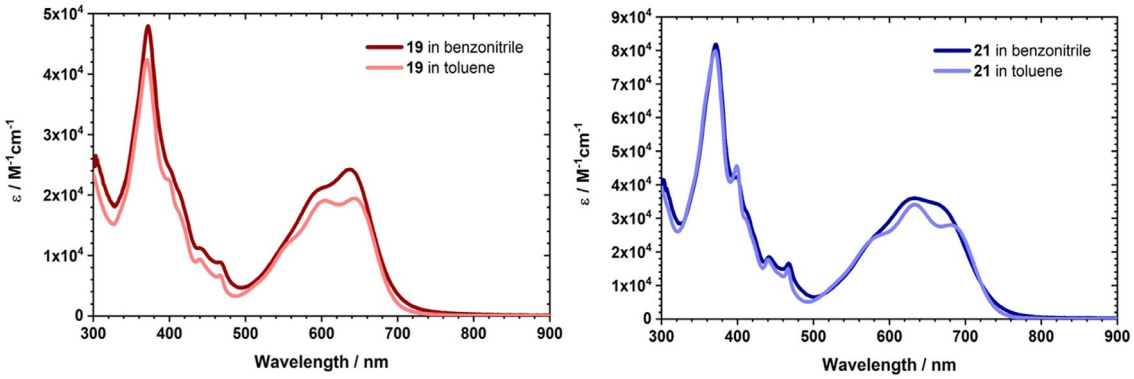

Figure 3. Steady-state absorption spectra of **19** ($c = 2\times10^{-6}$ M, left) and **21** ($c = 2\times10^{-6}$ M, right) in toluene and benzonitrile PhCN at room temperature.

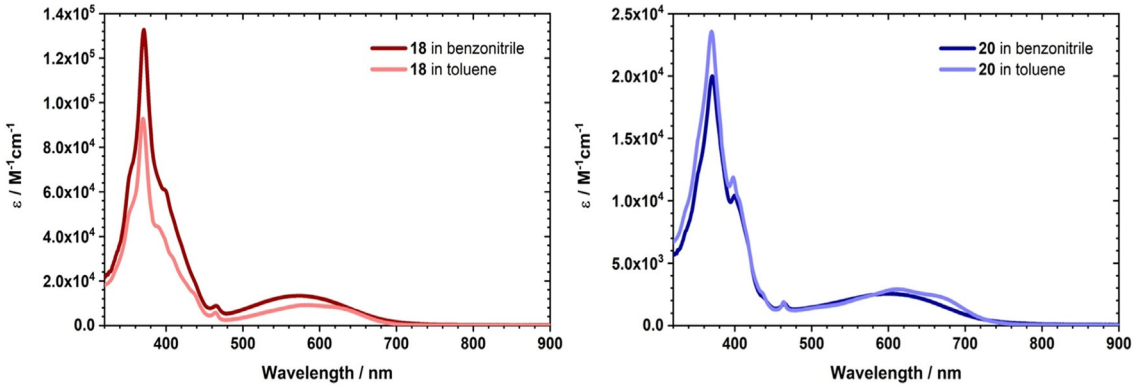

Figure 4. Steady-state absorption spectra of **18** ($c = 2\times10^{-6}$ M, left) and **20** ($c = 2\times10^{-6}$ M, right) in toluene and benzonitrile PhCN at room temperature.

absorptions of PDI at 558, 604, and 644 nm. Notably, a lower symmetry due to PDI-functionalization leads to an intensification of the symmetry-forbidden α-bands. In linear PDI–HBC **21**, all HBC-centered absorptions are identical to those seen for **19**. Only, the PDI absorptions are different. In particular, the high-energy absorption at 633 nm is higher in intensity than the low-energy absorption at 681 nm. At this point, we conclude that linear PDI–HBC **21** aggregates. In more polar PhCN, the HBC-centered absorptions show a red-shift of 1 nm, while the PDI-centered blue-shifts by 5–7 nm. This points towards a charge transfer character of the PDI ground states. The extinction coefficients of **19** and **21** range from 1×10^4 to 8×10^4 M^{-1} cm^{-1} and are higher in **21** than in **19** (Figure 3).

The absorption spectra of helical NDI–HBC **18** and linear NDI–HBC **20** display the HBC-features seen for **19** and **21**, respectively. Additionally, a broad, low-intense absorption is discernable between 470 and 750 nm, which shows a distinct polarity dependence, visible by a 10 nm blueshift when changing from non-polar toluene to highly polar PhCN (Figure 4). The extinction coefficient of **18** and **20** in toluene maximize at the β-band of HBC at 371 nm ranging from 2.3×10^4 to 9×10^4 M^{-1} cm^{-1}, whereby **18** possessing higher values than **20**. Switching to PhCN leads to an increase of the extinction for **18**, while it decreases in case of **20**.

Fluorescence properties

The fluorescence features of helical PDI–HBC **19** in toluene are dominated by a 692 nm maximum (Figure S49). Such a significant Stokes shift, that is, 48 nm, between the long-wavelength absorption at 644 nm and the short-wavelength fluorescence at 692 nm is rather unusual for PDIs. It is more likely that the fluorescence/emission stems from a different state: charge-transfer (CT) state. Notably, a weaker shoulder appears around 615 nm, indicating the presence of weak PDI centered fluorescence. In PhCN, the relative intensities are reversed. Now, a low-intense 615 nm feature dominates followed by a weaker one at 653 nm. Under these conditions, the CT emission is missing, leaving a weak PDI fluorescence behind. 3D fluorescence heat maps measurements of **19** indicate that a unidirectional energy transfer from HBC to PDI is responsible for the quantitative HBC fluorescence quenching in toluene and PhCN (Figure 5).

For linear PDI–HBC **21**, the changes between non-polar and polar solvent are less dramatic (Figure S49). In toluene, the major fluorescence maximum appears at 639 nm followed by a weaker fluorescence maximum, at 713 nm. From 3D fluorescence heat map measurements in toluene an interesting mechanism is concluded (Figure S50). HBC excitation at, for example, 370 nm leads to the PDI-related fluorescence at 640 nm next to the rather intense CT emission at 750 nm. In contrast,

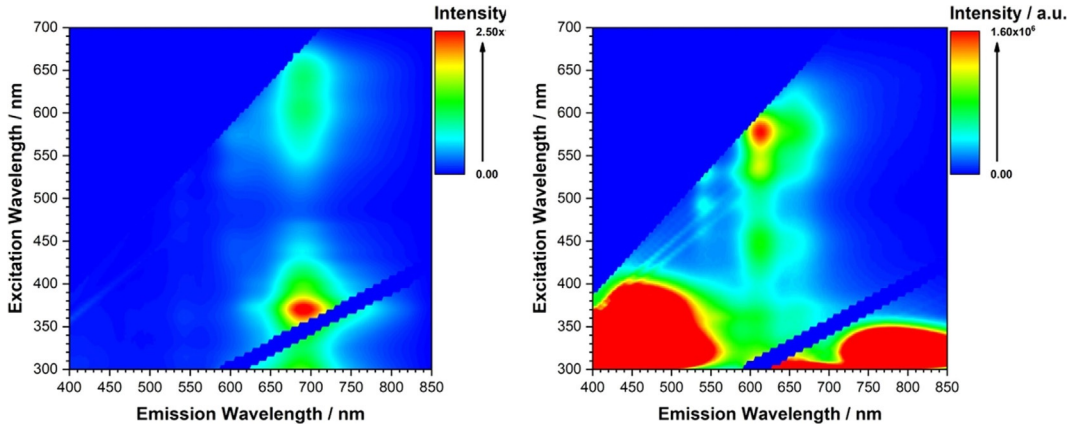

Figure 5. 3D fluorescence spectra of **19** ($c = 2 \times 10^{-6}$ M) in toluene (left) and PhCN (right) at room temperature.

CT emission is absent upon PDI excitation. Here, aggregation might be a possible explanation. In PhCN, only the PDI-centered fluorescence is noted at 645 nm.

The fluorescence quantum yields were determined using Oxazine 1 in ethanol as reference ($\phi_{Fl} = 14.1\,\%$). In toluene, the quantum yields for **19** and **21** are 18.7 % and 5.1 %, respectively. The lower quantum yield for **21** is ascribed to aggregation. In PhCN, the quantum yields are strongly quenched to 1.5 % and 2.3 % for **19** and **21**, respectively, indicating an alternative pathway of the excited state deactivation (Table S1).

The fluorescence of helical NDI–HBC **18** and linear NDI–HBC **20** is weak in toluene as well as PhCN. From the 3D fluorescence heat map measurements of **18** and **20** in toluene, we conclude that the 705 nm fluorescence is generated regardless of the excitation wavelength (Figure 6 and Figure S51). Stoke shifts as large as 50 nm and beyond points toward a radiative decay of a CT state. In the case of **20** and toluene, the fluorescence heat map is dominated by unstructured fluorescence including several local maxima between 500 and 650 nm. Switching to PhCN leads for helical NDI–HBC **18** and linear NDI–HBC **20** to a strongly quenched fluorescence. Determination of the fluorescence quantum yields failed with upper limits of 0.1 %.

Electrochemistry

All compounds were probed in DCM with 0.1 M $TBAPF_6$ as electrolyte. With the help of differential pulse and cyclic voltammetry, the reductions and oxidations as well as their reversibility were investigated. Notably, all processes are at least quasi-reversible if not reversible (Table S2).

For helical PDI–HBC **19**, HBC- and PDI-centered oxidations evolve at +0.59, +0.79, +1.08, and +0.67 V, respectively (all vs. Fc/Fc^+). In terms of reduction, only PDI-centered reductions are discernible at −1.19 and −1.35 V vs. Fc/Fc^+ (Figures S52 and S53). Linear PDI–HBC **21** gives rise to the same reductions. Different are, however, the oxidations. Additional oxidations are seen at +0.38 and +0.47 V. A reasonable rationale is based on the presence of aggregated **21** concluded in the steady state absorption measurements (see above; Figure 3).

In the case of helical NDI–HBC **18**, oxidations at +0.63 and +0.72 V vs. Fc/Fc^+ are HBC centered. Relative to helical PDI–HBC **19** all oxidations are shifted by the stronger electron accepting NDI. NDI lacks any appreciable oxidation within the range of up to 1.5 V, while reductions occur at −1.05, −1.37, and −1.48 V vs. Fc/Fc^+ (Figure S54 and Table S3). NDI in helical NDI–HBC **18** is the stronger electron acceptor when compared to PDI in helical PDI–HBC **19**.

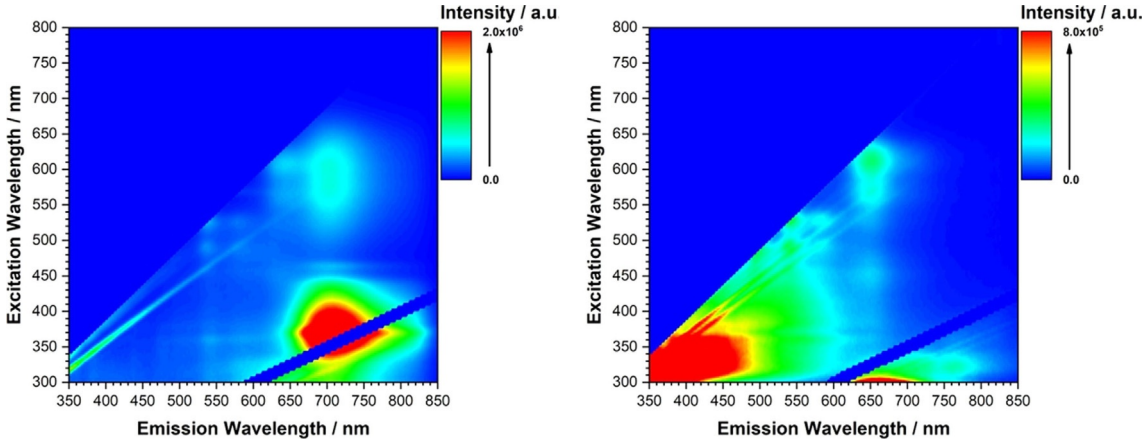

Figure 6. 3D fluorescence spectra of **18** ($c = 2 \times 10^{-6}$ M) in toluene (left) and PhCN (right) at room temperature.

Oxidations in linear NDI–HBC **20** are moderately shifted relative to those in helical NDI–HBC **18**. Once again, aggregation is responsible. Reductions in linear NDI–HBC **20** are not affected by aggregation. What changes, however, is the relative intensity ratio of the reductions. In helical NDI–HBC **18**, the −1.37 V reduction is best described as a feature superimposed to the −1.48 V reduction. This trend is reversed in linear NDI–HBC **20**.

Spectroelectrochemistry

The spectroelectrochemical reduction of **19** at −1.0 V caused significant changes in the absorption spectra. New 841 and 1029 nm absorptions evolve at the expense of 367, 599 and 633 nm absorptions. All of these changes relate to the spectral fingerprints of the one-electron reduced form of PDI (Figure S55).

For **18**, spectroelectrochemical reduction at −0.9 V led to lower intensities of the 367 and 571 nm absorption. The latter is replaced by a split absorption at 367 and 381 nm next to a broad absorption between 420 and 550 nm with local maxima at 468 and 513 nm (Figure S55).

Transient absorption spectroscopy

In transient absorption spectroscopy, we focused on the solvent dependence of excited state dynamics. Photoexciting **19** with 610 nm in toluene leads to instantaneous formation of excited-state absorptions at 489 and 986 nm together with bleaching between 550 and 800 nm. Hereby, minima at 600 and 700 nm relate to ground state bleaching and stimulated fluorescence, respectively. Within 100 ps the 986 nm transient blue-shifts by 10 nm before recovering the ground-state within 5500 ps (Figure S56). In PhCN, the blue-shift goes hand-in-hand with the evolution of new transients at 715 nm and at around 1050 nm (Figure 7). Furthermore, the blue-shift is with 50 nm stronger and the decay with several hundreds of picoseconds is distinctly accelerated. The transient features of **21** are similar albeit slightly shifted. In toluene, the excited-state absorptions maximize at 490 and 996 nm, while the bleaching minimizes at 628 and 709 nm (Figure S57). The latter blue-shifts with time by about 10 nm before reinstating the ground state. Measurements in PhCN differ in terms that a significantly faster ground-state recovery is seen as well as a 30 nm blue-shift of the 996 nm transient and the evolution of new transients at 750 nm and at around 1100 nm (Figure S58).

Via global analysis, all transient absorption measurements were fit with two species (Figure 7 and Figures S56–S58). Regardless of the solvent, the first species seen for **19** and **21** transforms within 7–15 ps into the second species. In line with the underlying blue-shift, this process is assigned to solvent and structural relaxation of a polar first singlet excited state with notable charge-transfer character.[12] Upon photoexcitation, this excited state is formed with the same solvation shell of the less polar ground state and is consequently in a highly strained configuration, which leads to a fast relaxation by rearranging its solvation shell and its structure. In toluene, we infer a notable charge transfer rather than charge-separated state character. Support for this notion came from the mismatch with the spectro-electrochemical data and the CT emission recorded in steady-state measurements (Figures S49 and S55). In PhCN, the initially populated state relaxes into a charge separated state. Here, the EAS spectra of the second species match the spectroelectrochemical data of the one-electron reduced **19** (Figure S55). It also coincides with the missing charge transfer emission. The charge separated state deactivation is significantly faster than the charge transfer deactivation with 130 ps and 1.82 ns for **19** and 91 and 439 ps for **21**, respectively. (Table S4).

Transient absorption measurements with **18** in toluene led to very different transients. For example, 610 nm photoexcitation is accompanied by a spectrum that lacks any bleaching. Instead, excited-state absorptions maximize at 457, 534, 702, 907, and 1356 nm (Figure S59). Important is the fact that in the following, the 1356 nm maximum blue-shifts by 60 nm and becomes less intense. In the case of **20**, immediate formation of maxima at 452, 502, 637, 714, 883, and 1017 nm are observed upon excitation (Figure S60). As time progresses, a slight blue-shift of most transients occurs followed by the complete deac-

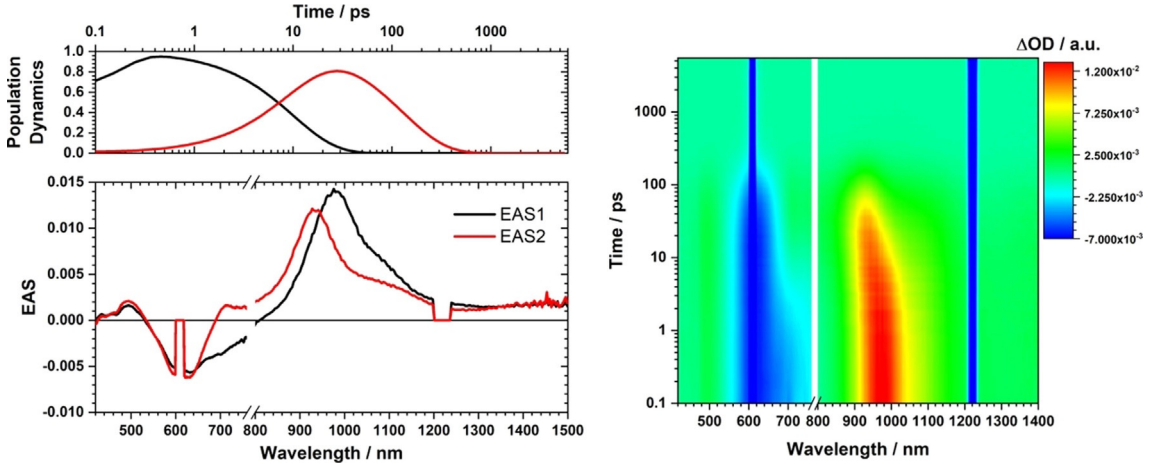

Figure 7. Evolution associated spectra with corresponding lifetime profiles (left) and chirp-corrected TA spectra of **19** ($c = 10^{-4}$ M) in PhCN at room temperature.

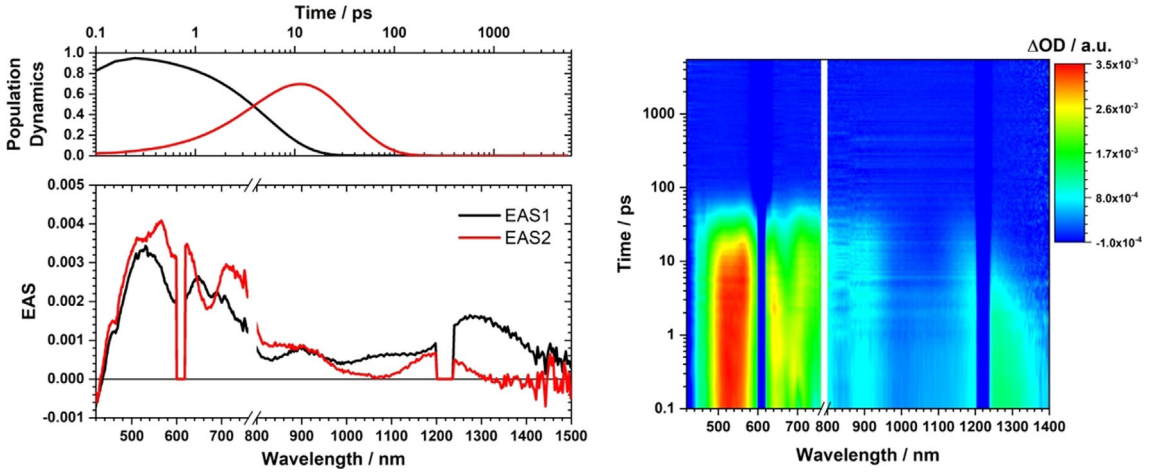

Figure 8. Evolution associated spectra with corresponding lifetime profiles (left) and chirp-corrected TA spectra of **18** ($c = 10^{-4}$ M) in PhCN at room temperature.

tivation to the ground state. In PhCN, the same sequence was noted for **18** and **20** (Figure 8 and Figure S61), whereby ground-state recovery takes place in less than 100 ps and the blueshifts of the transients at 1300 nm accounts for more than 80 nm.

In both solvents, the excited-state decays of **18** and **20** were fit biexponentially (Figure 8 and Figures S59–S61). The deactivation dynamics of **18** resemble those discussed for **19**. Photoexcitation at 610 nm leads to the population of an unrelaxed excited state with distinct charge transfer character. The large blueshifts of the features in non-polar toluene and polar PhCN suggest solvent relaxation. From here, ground state recovery occurs within 577 and 31 ps in toluene and PhCN, respectively. Again, we failed to detect spectral features that match those of the one-electron reduced form seen in spectroelectrochemical measurements (Figure S55). Therefore, we rule out the evolution of a charge-separated state. In toluene, the triplet excited state is weakly populated. For **20** in toluene, NDI stacking dictates a faster deactivation to afford the ground state within 362 ps (Table S5). The excited state deactivation of **20** in PhCN strongly resembles that summarized for **18** in PhCN.

Conclusions

The successful synthesis of helically and linearly fused naphthalenediimide (NDI)- and perylenediimide–hexa-*peri*-hexabenzocoronene (PDI–HBC) compounds is presented. The constitution of the product is determined, by which Br-isomer is used in the reaction sequence based of Diels–Alder and Scholl-type oxidation. Of great value is the selective formation of either a [5]-heterohelicene or a linear bridge as it allows insights into structure-property relations. At the forefront is the control over these fully conjugated, π-extended donor–acceptor systems (D–A). Photophysically, the strong coupling of the PDI/NDI with HBC reveal interesting results. The different conformations exert rather large effects on aggregation as, for example, seen in the steady-state absorption measurements. A linear arrangement such as in **20** and **21** enhances the π-conjugation. This, in turn, evokes red-shifted absorption and fluorescence features. All conjugates reveal charge-transfer (CT) character in the ground and excited states. For PDI–HBC compounds, the CT character of the ground state is based on a slightly hypsochromic shifted PDI absorption. For the NDI–HBC compounds, the evolution of a broad absorption suggests the existence of a CT in the ground state. CT emission points already in toluene to the strong electron withdrawing effects of rylenes in the excited state. Notable is the lack of any CT emission in high-polar PhCN. To this end, transient absorption experiments assisted in the elucidation of a deactivation via hot and relaxed CT states. The excited CT states of helical PDI–HBC **19** and linear PDI–HBC **21** transform into a charge-separated state and this transformation is a function of the solvent polarity. In the case of helical NDI–HBC **18** and linear NDI–HBC **20**, despite the lack of any CT emission in PhCN, no evidence was gathered for the involvement of a charge-separated state.

Experimental Section

Chemicals were purchased from Sigma–Aldrich and used without any further purification. Solvents were distilled prior to usage. Thin layer chromatography (TLC) was performed on Merck silica gel 60 F524, detected by UV-light (254 nm, 366 nm). Plug chromatography and column chromatography were performed on Macherey–Nagel silica gel 60 M (deactivated, 230–400 mesh, 0.04–0.063 mm). NMR spectra were recorded on a Bruker Avance 400 (^{1}H: 400 MHz, ^{13}C: 101 MHz), a Bruker Avance 500 (^{1}H: 500 MHz, ^{13}C: 126 MHz), or a Bruker Avance Neo Cryo-Probe DCH (^{1}H: 600 MHz, ^{13}C: 151 MHz). Deuterated solvents were purchased from Sigma–Aldrich and used as received. Chemical shifts are given in ppm at room temperature and are referenced to residual protic impurities in the solvents (^{1}H: $CHCl_3$: 7.24 ppm, CH_2Cl_2: 5.32 ppm, $C_2H_2Cl_4$: 5.91 ppm) or the deuterated solvent itself ($^{13}C\{^1H\}$: $CDCl_3$: 77.16 ppm, CD_2Cl_2: 53.40 ppm, $C_2D_2Cl_4$: 74.20 ppm). The resonance multiplicities are indicated as "s" (singlet), "brs" (broad singlet), "d" (doublet), "t" (triplet), "q" (quartet) and "m" (multiplet). Mass spectrometry was carried out with a Shimadzu AXIMA Confidence (MALDI-TOF, matrix: 2,5-dihydroxybenzoic acid DHB, *trans*-2-[3-(4-tert-butylphenyl)-2-methyl-2-propenyliden]malononitrile, DCTB) or without matrix (OM). High resolution mass spectrometry (HRMS) was recorded on a LDI/MALDI-ToF Bruker Ultraflex Extreme machine or on a APPI-ToF

mass spectrometer Bruker maXis 4G UHR MS/MS spectrometer. UV/Vis spectroscopy was carried out on a Varian Cary 5000 UV-vis-NIR spectrometer. The spectra were recorded at RT in DCM in quartz cuvettes (edge length = 1 cm) under ambient conditions. Fluorescence spectra were obtained from a Shimadzu RF-5301 PC and a NanoLog spectrofluorometer (Horiba Scientific). Steady-state absorption experiments were performed using a Lambda 2 spectrophotometer from PerkinElmer. The measurements were conducted in a 10 mm × 10 mm quartz cuvette. Steady-state fluorescence measurements were also carried out in a 10 mm × 10 mm quartz cuvette. The instruments were a FluoroMax®-3 fluorometer from Horiba Jovin Yvon equipped with a R928P photomultiplier tube from Hamamatsu (185 −850 nm) and a FS5 spectrofluorometer. Time-resolved absorption studies were performed using the Clark MXR CPA 2101 and CPA2110 Ti:sapphire amplifier (775 nm, 1 kHz,150 fs pulse width) as the laser source. An Ultrafast Systems HELIOS femtosecond transient absorption spectrometer was used to acquire time-resolved transient absorption spectra with 150 fs resolution and time delays from 0 to 5500 ps. The probe -visible white light (≈400–770 nm)- was generated by focusing a fraction of the fundamental 775 nm output onto a 2 mm sapphire disk. Also, for the (near) IR (780–1500 nm) determination, a 1 cm sapphire was used. A noncollinear optical parameter (NOPA, Clark MXR) was used to generate the excitation wavelength at 568 nm; a bandpass filter ±10 nm was used to exclude the fundamental 775 and 387 nm. All measurements were conducted in 2 mm quartz cuvettes under argon atmosphere. Electrochemical measurements were carried out with a three-electrode setup. A glassy carbon disk served as working electrode, an Ag/AgCl was used as reference electrode and a Pt-plate was used as counter electrode. Voltage was controlled with an EG&G Princeton Applied Research potentiostat. The data was recorded with NOVA 1.10 software. Spectro-electrochemistry was conducted with a home-made three neck cell in a Cary 5000 UV/Vis/NIR spectrometer from Varian and the respective processing software. We used a three-electrode setup consisting of a Pt-gauze as working electrode, a Pt-wire as counter electrode and a silver wire as pseudo reference electrode.

General procedure for the Sonogashira coupling reaction (GP I): A 5 mL microwave (MW) vial was charged with bromo-benzimidazole-rylene, $PdCl_2(PPh_3)_2$, CuI and toluene and sealed with a septum. The solution was degassed for 10 min and subsequently alkyne **8**[10] dissolved in Et_3N was added via syringe. The reaction mixture was stirred at 80 °C overnight under nitrogen atmosphere. The crude product was subjected to silica plug chromatography to provide the pure products.

General procedure for the Diels–Alder reaction (GP II): A 1 mL MW-vial was charged with rylene-tolan, tetracyclone **13**[11] and toluene and sealed with a septum. The reaction mixture was degassed with N_2 for 5 min and heated to 220 °C for 24 h. The solvent was removed under reduced pressure and the crude was purified by plug chromatography to provide the pure products.

General procedure for the Scholl oxidation (GP III): In a MW-vial Rylene-HPB was dissolved in DCM and cooled to 0 °C with an ice bath. After degassing with N_2 for 20 min a solution of dry $FeCl_3$ in $MeNO_2$ was added. The mixture was degassed for further 15 min and stirred overnight. The reaction was quenched via the addition of MeOH. The solvent was removed under reduced pressure and the crude product was purified by plug chromatography to provide the pure products.

4- and 5-Br-1,2-naphthaleneimidebenzimidazole (4 and 6): A dry flask was charged with NMI **2** (100 mg, 0.237 mmol, 1.1 equiv.), 4-bromo-1,2-diaminbenzene **1** (40.0 mg, 0.216 mmol, 1 equiv.) and imidazole (800 mg) and the mixture was stirred under nitrogen at 160 °C for 3 h. The reaction mixture was cooled to RT, dissolved in DCM and washed with H_2O. The combined organic layers were concentrated under reduced pressure and the crude was purified by silica gel column chromatography (SiO_2, DCM/hexanes 1:1) to provide the two separated isomers **4** and **6** in a pure form. Yields: **4** (44.0 mg, 0.077 mmol, 36%), **6** (52.0 mg, 0.091 mmol, 42%).

*4-Br-1,2-naphthaleneimidebenzimidazole (**4**)*: ^{1}H NMR ($CDCl_3$, 400 MHz, 25 °C): δ = 8.87–8.66 (m, 4H, Ar-CH), 8.54 (d, J = 1.8 Hz, 1H, Ar-CH), 7.64 (d, J = 8.6 Hz, 1H, Ar-CH), 7.51 (dd, J = 8.6, 1.9 Hz, 1H, Ar-CH), 5.37–5.01 (m, 1H, *N*-CH), 2.29–2.17 (m, 2H, CH_2), 1.96–1.67 (m, 2H, CH_2), 1.42–1.05 (m, 12H, CH_2), 0.92–0.68 ppm (m, 6H, CH_3). ^{13}C NMR ($CDCl_3$, 101 MHz 25 °C): δ = 159.3 (C=O), 148.3, 143.0, 132.9 (Ar-C), 131.6, 130.0 (Ar-CH), 127.7 (Ar-C), 127.1 (Ar-CH), 126.9, 125.9, 125.1 (Ar-C), 121.9 (Ar-CH), 120.5 (Ar-C), 119.1 (Ar-CH), 55.4 (*N*-CH), 32.4, 31.8, 26.8, 22.7 (CH_2), 14.2 ppm (CH_3). MS (MALDI-TOF, dctb): m/z = 572.1663 ($C_{31}H_{31}BrN_3O_3$ $[M+H]^+$). HRMS: (APPI, CH_2Cl_2): calculated for $C_{31}H_{31}BrN_3O_3$ ($[M+H]^+$) m/z = 572.1543, found m/z = 572.1545. UV/Vis (CH_2Cl_2): λ [nm] (ε [M^{-1} cm^{-1}]) = 304 (23500), 316 (26500), 443 (18500). Fluorescence (CH_2Cl_2): $\lambda_{exc.}$ [nm] = 443, $\lambda_{emission}$ [nm] (rel. int.) = 570 (100).

*5-Br-1,2-naphthaleneimidebenzimidazole (**6**)*: ^{1}H NMR ($CDCl_3$, 400 MHz, 25 °C): δ = 8.97–8.56 (m, 4H, Ar-CH), 8.24 (d, J = 8.5 Hz, 1H, Ar-CH), 7.83 (d, J = 1.8 Hz, 1H, Ar-CH), 7.47 (dd, J = 8.7, 1.8 Hz, 1H. Ar-CH), 5.33–4.98 (m, 1H, *N*-CH), 2.34–2.11 (m, 2H, CH_2), 2.05–1.69 (m, 2H, CH_2), 1.41–0.96 (m, 12H, CH_2), 0.93–0.51 ppm (m, 6H, CH_3). ^{13}C NMR ($CDCl_3$, 101 MHz 25 °C): δ = 159.1 (C=O), 148.8, 145.2 (Ar-C), 131.6 (Ar-CH), 130.9 (Ar-C), 129.8 (Ar-CH), 127.6 (Ar-C), 127.2 (Ar-CH), 126.8, 125.8, 124.8 (Ar-C), 123.7 (Ar-CH), 119.7 (Ar-C), 116.9 (Ar-CH), 55.4 (*N*-CH), 32.4, 31.8, 26.8, 22.7 (CH_2), 14.2 ppm (CH_3). MS (MALDI-TOF, dctb): m/z = 572.2372 ($C_{31}H_{31}BrN_3O_3$ $[M+H]^+$). HRMS: (MALDI-TOF, dctb): calculated for $C_{31}H_{31}BrN_3O_3$ ($[M+H]^+$) m/z = 572.1543, found m/z = 572.1528. UV/Vis (CH_2Cl_2): λ [nm] (ε [M^{-1} cm^{-1}]) = 300 (22500), 312 (25500), 420 (16000). Fluorescence (CH_2Cl_2): $\lambda_{exc.}$ [nm] = 420, $\lambda_{emission}$ [nm] (rel. int.) = 556 (100).

Naphthalene-tolane I (9): **9** was prepared according to GP I: 4-Br-1,2-naphthaleneimidebenzimidazole **4** (100 mg, 176 μmol, 1 equiv.), $PdCl_2(PPh_3)_2$ (6.2 mg, 9.0 μmol, 0.05 equiv.), CuI (0.8 mg, 4.4 μmol, 0.02 equiv.), toluene (4 mL), 1-(*tert*-butyl)-4-ethynylbenzene **8** (42.0 mg, 264 μmol, 1.5 equiv.), Et_2N (2 mL); plug chromatography (SiO_2, DCM/hexanes 1:1); yield (red solid) 60% (69.0 mg, 106 μmol). ^{1}H NMR ($CDCl_3$, 400 MHz, 25 °C): δ = 9.00–8.69 (m, 4H, Ar-CH), 8.65 (d, J = 1.4 Hz, 1H, Ar-CH), 7.84 (d, J = 8.3 Hz, 1H, Ar-CH), 7.61 (dd, J = 8.4, 1.6 Hz, 1H, Ar-CH), 7.54–7.45 (m, 2H, Ar-CH), 7.45–7.34 (m, 2H, Ar-CH), 5.16 (m, 1H, *N*-CH), 2.32–2.07 (m, 2H, CH_2), 2.01–1.73 (m, 1H, CH_2), 1.34 (s, 9H, CH_3), 1.32–1.17 (m, 12H, CH_2), 0.88–0.61 pp (m, 6H, CH_3). ^{13}C NMR ($CDCl_3$, 101 MHz 25 °C): δ = 159.4 (C=O), 152.1, 148.6, 143.4, 132.0, 131.6, 130.4, 127.8, 127.1, 125.9, 125.6, 122.5, 120.7, 120.1, 119.1 (Ar-CH, Ar-C), 91.5, 89.0 (C≡C), 55.4 (*N*-CH), 35.0, 32.4, 31.8, 31.3, 26.8, 22.7, 14.2 ppm (CH_3, CH_2, C). MS (MALDI-TOF, dctb): m/z = 649.4343 ($C_{43}H_{43}N_3O_3$ $[M+H]^+$). HRMS: (MALDI-TOF, dctb): calculated for $C_{43}H_{43}N_3O_3$ ($[M+H]^+$) m/z = 649.3299, found m/z = 649.3308. UV/Vis (CH_2Cl_2): λ [nm] (ε [M^{-1} cm^{-1}]) = 326 (31000), 480 (14000).

Naphthalene-tolane II (11): **11** was prepared according to GP I: 5-Br-1,2-naphthaleneimidebenzimidazole **6** (30 mg, 53 μmol, 1 equiv.), $PdCl_2(PPh_3)_2$ (1.9 mg, 2.7 μmol, 0.05 equiv.), CuI (0.2 mg, 1.1 μmol, 0.02 equiv.), toluene (2 mL), 1-(*tert*-butyl)-4-ethynylbenzene 8 (17 mg, 0.11 mmol 2 equiv.), Et_2N (1 mL); plug chromatography (SiO_2, DCM/hexanes 1:1); yield (red solid) 76% (26 mg, 40 μmol). ^{1}H NMR ($CDCl_3$, 400 MHz, 25 °C): δ = 8.97–8.68 (m, 4H, Ar-CH), 8.43 (d, J = 8.3 Hz, 1H, Ar-CH), 7.99 (d, J = 1.4 Hz, 1H, Ar-CH), 7.65 (dd, J = 8.4, 1.5 Hz, 1H, Ar-CH), 7.55–7.46 (m, 2H, Ar-CH), 7.43–7.33 (m, 2H, Ar-CH), 5.25–5.09 (m, 1H, *N*-CH), 2.30–2.11 (m, 2H,

CH_2), 1.93–1.73 (m, 2H, CH_2), 1.33 (s, 9H, CH_3), 1.31–1.19 (m, 12H, CH_2), 0.94–0.65 ppm (m, 6H, CH_3). ^{13}C NMR ($CDCl_3$, 101 MHz 25 °C): δ = 159.3 (C=O), 152.0, 148.8, 144.1, 144.0, 131.8, 131.6, 131.5, 130.6, 129.9, 127.7, 127.7, 127.1, 125.9, 125.6, 125.3, 123.9, 122.1, 120.1, 115.9 (Ar-CH, Ar-C), 90.3, 88.5 (C≡C), 55.4 (*N*-CH), 35.0, 32.4, 31.8, 31.4, 26.8, 22.7, 14.2 ppm (CH_3, CH_2, C). MS (MALDI-TOF, dctb): *m/z* = 650.3641 ($C_{43}H_{43}N_3O_3$ [M+H]$^+$). HRMS: (APPI, CH_2Cl_2): calculated for $C_{43}H_{43}N_3O_3$ ([M+H]$^+$) *m/z* = 649.3299, found *m/z* = 649.3299. UV/Vis (CH_2Cl_2): λ [nm] (ε [M^{-1} cm^{-1}]) = 321 (25000), 418 (10000).

Helical NDI–HPB (14): **14** was prepared according to GP II: naphthalene-tolane **9** (30 mg, 46 µmol, 1 equiv.), tetracyclone **13** (28 mg, 46 µmol, 1 equiv.), toluene (0.75 mL); plug chromatography (SiO_2, DCM/hexanes 1:1); yield (red solid) 58% (33 mg, 27 µmol). ^{1}H NMR ($CDCl_3$, 400 MHz, 25 °C): δ = 8.76–8.52 (m, 4H, Ar-CH), 8.01 (d, *J* = 1.5 Hz, 1H, Ar-CH), 7.36 (d, *J* = 8.3 Hz, 1H, Ar-CH), 7.05 (dd, *J* = 8.4, 1.6 Hz, 1H, Ar-CH), 6.86–6.65 (m, 20H, Ar-CH), 5.24–5.01 (m, 1H, *N*-CH), 2.30–2.09 (m, 2H, CH_2), 1.92–1.72 (m, 2H, CH_2), 1.35–1.16 (m, 12H, CH_2), 1.12–1.06 (m, 27H, CH_3), 0.96 (s, 18H, CH_3), 0.84–0.76 ppm (m, 6H, CH_3). ^{13}C NMR ($CDCl_3$, 101 MHz 25 °C): δ = 158.7 (C=O), 147.8, 147.7, 147.6, 147.4, 141.6, 141.2, 141.2, 140.9, 140.5, 139.3, 137.9, 137.9, 131.5, 131.2, 131.1, 131.1, 131.0, 130.8, 129.4, 129.3, 127.6, 127.4, 126.1, 125.9, 125.8, 125.7, 125.6, 123.6, 123.4, 123.2, 119.2, 118.7 (Ar-CH, Ar-C), 55.3 (*N*-CH), 34.2, 34.2, 34.2, 32.4, 31.9, 31.3, 31.2, 26.7, 22.7, 14.2 ppm (CH_3, CH_2, C). MS (MALDI-TOF, dctb): *m/z* = 1230.9965 ($C_{87}H_{95}N_3O_3$ [M]$^+$). HRMS: (MALDI-TOF, dctb): calculated for $C_{87}H_{95}N_3O_3$ ([M]$^+$) *m/z* = 1229.7368, found *m/z* = 1229.7338. UV/Vis (CH_2Cl_2): λ [nm] (ε [M^{-1} cm^{-1}]) = 483 (12200).

Linear NDI–HPB (16): **16** was prepared according to GP II: naphthalene-tolane **11** (22 mg, 34 µmol, 1 equiv.), tetracyclone **13** (21 mg, 34 µmol, 1 equiv.), toluene (0.5 mL); plug chromatography (SiO_2, DCM/hexanes 1:1); yield (orange solid) 79% (33 mg, 27 µmol). ^{1}H NMR ($CDCl_3$, 400 MHz, 25 °C): δ = 8.71–8.47 (m, 4H, Ar-CH), 7.98 (d, *J* = 8.3 Hz, 1H, Ar-CH), 7.44 (d, *J* = 1.6 Hz, 1H, Ar-CH), 7.13 (dd, *J* = 8.4, 1.5 Hz, 1H, Ar-CH), 6.86–6.61 (m, 20H Ar-CH), 5.14 (m, 1H, *N*-CH), 2.20 (m, 2H, CH_2), 1.89–1.76 (m, 2H, CH_2), 1.34–1.18 (m, 12H, CH_2), 1.08 (m, 27H, CH_3), 0.99 (s, 18H, CH_3), 0.83–0.76 ppm (m, 6H, CH_3). ^{13}C NMR ($CDCl_3$, 101 MHz, 25 °C): δ = 159.0 (C=O), 147.6, 147.5, 147.4, 147.2, 142.9, 140.9, 140.8, 140.4, 140.3, 138.9, 137.8, 137.8, 137.6, 131.3, 131.2, 131.0, 130.9, 129.5, 127.4, 127.3, 126.1, 125.5, 123.7, 123.5, 123.3, 123.1, 123.0, 113.8 (Ar-CH, Ar-C), 55.1 (*N*-CH), 34.1, 34.0, 32.3, 31.7, 31.3, 31.2, 31.1, 26.6, 22.5, 14.0 ppm (CH_3, CH_2, C). MS (MALDI-TOF, dctb): *m/z* = 1230.9766 ($C_{87}H_{95}N_3O_3$ [M]$^+$). HRMS: (MALDI-TOF, dctb): calculated for $C_{87}H_{96}N_3O_3$ ([M+H]$^+$) *m/z* = 1230.7446, found *m/z* = 1230.7494. UV/Vis (CH_2Cl_2): λ [nm] (ε [M^{-1} cm^{-1}]) = 435 (13500).

Helical NDI–HBC (18): **18** was prepared according to GP III: helical NDI–HPB **14** (23 mg, 19 µmol, 1 equiv.), DCM (20 mL), dry $FeCl_3$ (49 mg, 0.30 mmol, 16 equiv.) $MeNO_2$ (0.2 mL); plug chromatography (SiO_2, DCM/hexanes 1:1); yield (blue/green solid) 88% (20 mg, 17 µmol). ^{1}H NMR ($C_2D_2Cl_4$, 500 MHz, 90 °C): δ = 9.81 (s, 1H, Ar-CH), 9.45 (d, *J* = 1.7 Hz, 1H, Ar-CH), 9.41–9.27 (m, 8H, Ar-CH), 9.16 (d, *J* = 7.6 Hz, 1H, Ar-CH), 8.85 (d, *J* = 7.6 Hz, 1H, Ar-CH), 8.80 (d, *J* = 1.4 Hz, 2H, Ar-CH), 8.45 (d, *J* = 1.7 Hz, 1H, Ar-CH), 5.23–5.13 (m, 1H, *N*-CH), 2.30–2.18 (m, 2H, CH_2), 1.92 (m, 2H, CH_2), 1.85 (s, 9H, CH_3), 1.84 (s, 9H, CH_3), 1.83 (s, 9H, CH_3), 1.82 (s, 9H, CH_3), 1.61 (s, 9H, CH_3), 1.40–1.24 (m, 12H, CH_2), 0.86 ppm (m, 6H, CH_3). ^{13}C NMR ($CDCl_3$, 151 MHz, 25 °C): δ = 154.8 (C=O), 147.8, 146.5, 146.5, 146.4, 146.3, 143.9, 141.8, 128.7, 128.3, 127.9, 127.8, 127.7, 127.7, 127.6, 127.6, 127.5, 126.9, 126.4, 126.4, 125.6, 125.5, 124.8, 123.9, 123.9, 123.7, 123.5, 123.2, 123.0, 122.8, 122.4, 121.0, 121.0, 120.8, 120.7, 118.7, 118.4, 117.9, 117.9, 117.8, 117.5, 117.3, 116.8, 116.8, 116.6, 116.6, 116.3, 116.2, 115.9, 110.9 (Ar-CH, Ar-C), 52.4 (*N*-CH), 32.99, 32.99, 32.98, 32.9, 32.7, 29.5, 29.3, 29.24, 29.22, 29.0, 28.9, 23.9, 23.8, 19.79, 19.78, 11.3 ppm (CH_3, CH_2, C). MS (MALDI-TOF, dctb): *m/z* = 1217.6478 ($C_{87}H_{83}N_3O_3$ [M]$^+$). HRMS: (MALDI-TOF, dctb): calculated for $C_{87}H_{83}N_3O_3$ ([M]$^+$) *m/z* = 1217.6429, found *m/z* = 1217.6419. UV/Vis (CH_2Cl_2): λ [nm] (ε [M^{-1} cm^{-1}]) = 368 (125000), 576 (11800).

Linear NDI–HBC (20): **20** was prepared according to GP III: linear NDI–HPB **16** (27 mg, 22 µmol, 1 equiv.), DCM (20 mL), dry $FeCl_3$ (57 mg, 0.35 mmol, 16 equiv.) $MeNO_2$ (0.2 mL); plug chromatography (SiO_2, DCM/hexanes 1:1); yield (green solid) 85% (17 mg, 8.7 µmol). ^{1}H NMR ([D_8]toluene, 400 MHz, 100 °C): δ = 10.97 (s, 1H, Ar-CH), 9.98 (s, 1H, Ar-CH), 9.60–9.25 (m, 9H, Ar-CH), 8.38–8.36 (m, 1H, Ar-CH), 8.27–8.25 (m, 1H, Ar-CH), 7.96–7.92 (m, 1H, Ar-CH), 7.79–7.74 (m, 1H, Ar-CH), 5.46–5.31 (m, 1H, *N*-CH), 2.54–2.41 (m, 2H, CH_2), 2.23–2.17 (m, 2H, CH_2), 2.04 (s, 9H, CH_3), 1.97 (s, 9H, CH_3), 1.91 (m, 18H, CH_3), 1.89 (s, 9H, CH_3), 1.40–1.26 (m, 12H, CH_2), 0.99–0.88 ppm (m, 6H, CH_3). HRMS: (APPI, CH_2Cl_2): calculated for $C_{87}H_{84}N_3O_3$ ([M+H]$^+$) *m/z* = 1218.6507, found *m/z* = 1218.6503. UV/Vis (CH_2Cl_2): λ [nm] (qualitative) = 368, 606.

4- and 5-Br-1,2-peryleneimidebenzimidazole (5 and 7): A dry flask was charged with PMI **3** (150 mg, 0.132 mmol, 1.1 equiv.), 4-bromo-1,2-diaminobenzene **1** (22.0 mg, 0.120 mmol, 1 equiv.) and imidazole (800 mg) and the mixture was stirred under nitrogen at 120 °C for 1 h. The reaction mixtures was cooled to RT, dissolved in DCM and washed with H_2O. The combined organic layers were concentrated under reduced pressure and the crude was purified by silica gel plug chromatography (SiO_2, DCM/hexanes 3:7) to provide the two separated isomers **5** and **7** in a pure form. Yields: **5** (37.0 mg, 0.029 mmol, 24%), **7** (45.0 mg, 0.035 mmol, 29%).

*4-Br-1,2-peryleneimidebenzimidazole (**5**)*: ^{1}H NMR (CD_2Cl_2, 400 MHz, 25 °C): δ = 8.60 (d, *J* = 1.8 Hz, 1H, Ar-CH), 8.41–8.28 (m, 2H, Ar-CH), 8.14–8.02 (m, 2H, Ar-CH), 7.58 (d, *J* = 8.5 Hz, 1H, Ar-CH), 7.52 (dd, *J* = 8.6, 1.9 Hz, 1H, Ar-CH), 7.38–7.23 (m, 8H, Ar-CH), 7.00–6.91 (m, 2H, Ar-CH), 6.89–6.77 (m, 6H, Ar-CH), 5.14–5.01 (m, 2H, *N*-CH), 2.23–2.05 (m, 2H, CH_2), 1.84–1.67 (m, 2H, CH_2), 1.34 (s, 9H, CH_3), 1.32–1.30 (m, 27H, CH_3), 1.28–1.18 (m, 12H, CH_2), 0.88–0.77 (m, 6H, CH_3) ppm. ^{13}C NMR (CD_2Cl_2, 101 MHz, 25 °C): δ = 160.1 (C=O), 156.8, 156.5, 156.4, 156.0, 153.74, 153.71, 153.6, 153.5, 149.5, 148.1, 148.0, 147.96, 147.92, 143.5, 134.2, 133.3, 132.7, 129.6, 127.3, 127.23, 127.20, 122.9, 122.8, 121.7, 121.1, 120.9, 120.1, 120.0, 119.9, 119.8, 119.5, 119.3, 119.2, 116.6 (Ar-CH, Ar-C), 55.1 (*N*-CH), 34.89, 34.85, 32.9, 32.3, 31.82, 31.78, 31.76, 27.1, 23.2, 14.4 (CH_3, CH_2, C) ppm. MS (MALDI-TOF, dctb): *m/z* = 1289.6465 ($C_{81}H_{82}BrN_3O_7$ [M]$^+$). HRMS: (MALDI-TOF, dctb): calculated for $C_{81}H_{82}BrN_3O_7$ ([M]$^+$) *m/z* = 1287.5331, found *m/z* = 1287.5309. UV/Vis (CH_2Cl_2): λ [nm] (ε [M^{-1} cm^{-1}]) = 453 (16500), 567 (36500), 610 (57500). Fluorescence (CH_2Cl_2): $\lambda_{exc.}$ [nm] = 610, $\lambda_{emission}$ [nm] (rel. int.) = 649 (100).

*5-Br-1,2-peryleneimidebenzimidazole (**7**)*: ^{1}H NMR (CD_2Cl_2, 400 MHz, 25 °C): δ = 8.35–8.33 (m, 2H, Ar-CH), 8.29 (d, *J* = 8.6 Hz, 1H, Ar-CH), 8.17–8.04 (m, 2H, Ar-Ch), 7.86 (d, *J* = 1.8 Hz, 1H, Ar-CH), 7.50 (dd, *J* = 8.5, 1.9 Hz, 1H, Ar-CH), 7.36–7.26 (m, 8H, Ar-CH), 7.10–7.04 (m, 1H, Ar-CH), 6.96–6.81 (m, 7H, Ar-CH), 5.21–4.83 (m, 1H, *N*-CH), 2.22–2.08 (m, 2H, CH_2), 1.80–1.68 (m, 2H, CH_2), 1.34 (s, 9H, CH_3), 1.32–1.30 (m, 27H, CH_3), 1.28–1.21 (m, 12H, CH_2), 0.92–0.79 ppm (m, 6H, CH_3). ^{13}C NMR (CD_2Cl_2, 101 MHz, 25 °C): δ = 160.1 (C=O), 156.8, 156.5, 156.1, 153.8, 153.7, 153.6, 153.5, 150.4, 150.1, 148.1, 148.0, 147.9, 145.8, 134.2, 132.68, 131.4, 129.8, 128.9, 127.3, 127.24, 127.21, 126.1, 123.4, 123.0, 122.8, 121.1, 120.7, 120.1, 120.0, 119.9, 119.6, 119.33, 119.30, 117.3, 116.8 (Ar-CH, Ar-C), 55.1 (*N*-CH), 34.89, 34.86, 32.9, 32.3, 31.81, 31.78, 31.77, 27.1, 23.1, 14.4 ppm (CH_3, CH_2, C). MS (MALDI-TOF, dctb): *m/z* = 1289.5334 ($C_{81}H_{82}BrN_3O_7$ [M]$^+$). HRMS: (MALDI-TOF, dctb): calculated for $C_{81}H_{82}BrN_3O_7$ ([M]$^+$) *m/z* = 1287.5331, found *m/z* = 1287.5311. UV/Vis (CH_2Cl_2): λ [nm] (ε

[M^{-1} cm^{-1}]) = 445(11500), 566 (25500), 609 (41000). Fluorescence (CH_2Cl_2): $\lambda_{exc.}$ [nm] = 609, $\lambda_{emission}$ [nm] (rel. int.) = 648 (100).

Perylene-tolane I (10): **10** was prepared according to GP I: 4-Br-1,2-peryleneimidebenzimidazole **5** (20 mg, 16 μmol, 1 equiv.), $PdCl_2(PPh_3)_2$ (0.6 mg, 0.8 μmol, 0.05 equiv.), CuI (0.1 mg, 0.3 μmol, 0.02 equiv.), toluene (2 mL), 1-(*tert*-butyl)-4-ethynylbenzene **8** (3.7 mg, 23 μmol, 1.5 equiv.), Et_2N (1 mL); plug chromatography (SiO_2, DCM/hexanes 3:7); yield (blue solid) 100% (22 mg, 16 μmol). ^{1}H NMR (CD_2Cl_2, 400 MHz, 25 °C): δ = 8.54 (s, 1H, Ar-CH), 8.42–8.30 (m, 2H, Ar-CH), 8.20–8.03 (m, 2H, Ar-CH), 7.68 (d, J = 8.3 Hz, 1H, Ar-CH), 7.53 (d, J = 8.3 Hz, 1H, Ar-CH), 7.46–7.26 (m, 12H, Ar-CH), 6.99–6.81 (m, 8H, Ar-CH), 5.13–5.01 (m, 1H, *N*-CH), 2.20–2.07 (m, 2H, CH_2), 1.83–1.68 (m, 2H, CH_2), 1.34 (s, 9H, CH_3), 1.33–1.31 (m, 36H, CH_3), 1.26–1.19 (m, 12H, CH_2), 0.87–0.78 ppm (m, 6H, CH_3). ^{13}C NMR (CD_2Cl_2, 101 MHz, 25 °C): δ = 168.1 (C=O), 160.3, 156.8, 156.6, 156.3, 153.9, 153.8, 152.4, 150.0, 148.1, 148.0, 147.98, 144.4, 134.3, 133.1, 132.7, 132.4, 131.8, 131.5, 130.0, 129.3, 127.3, 127.25, 127.22, 126.0, 123.3, 122.6, 121.1, 121.0, 120.9, 120.6, 120.5, 120.2, 120.0, 119.9, 119.8, 119.4, 119.2, 116.6 (Ar-CH, Ar-C), 90.8, 89.7 (C≡C), 55.1 (*N*-CH), 35.3, 34.90, 34.87, 32.9, 32.3, 31.82, 31.79, 31.5, 30.3, 27.1, 23.1, 14.4 ppm (CH_3, CH_2, C). MS (MALDI-TOF, dctb): m/z = 1366.9423 ($C_{93}H_{95}N_3O_7$ ([M]$^+$). HRMS: (MALDI-TOF, dctb): calculated for $C_{93}H_{95}N_3O_7$ ([M]$^+$) m/z = 1365.7165, found m/z = 1365.7137. UV/Vis (CH_2Cl_2): λ [nm] (ε [M^{-1} cm^{-1}]) = 452 (11000), 577 (27000), 618 (39500). Fluorescence (CH_2Cl_2): $\lambda_{exc.}$ [nm] = 618, $\lambda_{emission}$ [nm] (rel. int.) = 655 (100).

Perylene-tolane II (12): **12** was prepared according to GP I: 5-Br-1,2-peryleneimidebenzimidazole **7** (40 mg, 31 μmol, 1 equiv.), $PdCl_2(PPh_3)_2$ (1.1 mg, 1.6 μmol, 0.05 equiv.), CuI (0.1 mg, 0.3 μmol, 0.02 equiv.), toluene (2 mL), 1-(*tert*-butyl)-4-ethynylbenzene **8** (7.4 mg, 46 μmol, 1.5 equiv.), Et_2N (1 mL); plug chromatography (SiO_2, DCM/hexanes 3:7); yield (blue solid) 92% (39 mg, 28 μmol). ^{1}H NMR (CD_2Cl_2, 500 MHz, 25 °C): δ = 8.39–8.32 (m, 3H, Ar-CH), 8.14–8.06 (m, 2H, Ar-CH), 7.81 (s, 1H, Ar-CH), 7.52 (dd, J = 8.4, 1.5 Hz, 1H, Ar-CH), 7.43–7.38 (m, 2H, Ar-CH), 7.37–7.24 (m, 10H, Ar-CH), 6.99–6.79 (m, 8H, Ar-CH), 5.12–5.02 (m, 1H, *N*-CH), 2.18–2.11 (m, 2H, CH_2), 1.79–1.72 (m, 2H, CH_2), 1.35 (s, 9H, CH_3), 1.32 (m, 18H, CH_3), 1.31 (s, 9H, CH_3), 1.30 (s, 9H, CH_3), 1.28–1.18 (m, 12H, CH_2), 0.83–0.80 ppm (m, 6H, CH_3). ^{13}C NMR (CD_2Cl_2, 126 MHz, 25 °C): δ = 165.0, 163.9 (C=O), 160.2, 156.8, 156.5, 156.4, 156.2, 153.9, 153.7, 153.6, 153.5, 152.3, 150.0, 148.0, 147.97, 147.95, 144.4, 134.2, 132.7, 132.2, 131.8, 129.8, 129.5, 127.29, 127.26, 127.2, 126.1, 125.9, 123.4, 123.2, 122.6, 121.3, 121.1, 120.9, 120.5, 120.2, 120.0, 119.9, 119.8, 119.7, 119.3, 116.7, 116.1 (Ar-CH, Ar-C), 90.0, 89.2 (C≡C), 55.1 (*N*-CH), 35.2, 34.90, 34.86, 32.9, 32.3, 31.83, 31.79, 31.78, 31.4, 27.1, 23.2, 14.4 ppm (CH_3, CH_2, C). MS (MALDI-TOF, dctb): m/z = 1366.7489 ($C_{93}H_{95}N_3O_7$ ([M]$^+$). HRMS: (MALDI-TOF, dctb): calculated for $C_{93}H_{95}N_3O_7$ ([M]$^+$) m/z = 1365.7165, found m/z = 1365.7183. UV/Vis (CH_2Cl_2): λ [nm] (ε [M^{-1} cm^{-1}]) = 452 (13000), 566 (31000), 609 (49500). Fluorescence (CH_2Cl_2): $\lambda_{exc.}$ [nm] = 609, $\lambda_{emission}$ [nm] (rel. int.) = 646 (100).

Helical PDI–HPB (15): **15** was prepared according to GP II: Perylene-tolan **10** (20 mg, 15 μmol, 1 equiv.), tetracyclone **13** (9 mg, 15 μmol, 1 equiv.), toluene (0.5 mL); plug chromatography (SiO_2, DCM/hexanes 3:7); yield (blue solid) 49% (14 mg, 7.2 μmol). ^{1}H NMR (CD_2Cl_2, 500 MHz, 25 °C): δ = 8.28–8.25 (m, 2H, Ar-CH), 8.15–8.04 (m, 2H, Ar-CH), 7.91 (dd, J = 1.6, 0.7 Hz, 1H, Ar-CH), 7.34–7.25 (m, 8H, Ar-CH), 7.24 (d, J = 8.3 Hz, 1H, Ar-CH), 6.96 (dd, J = 8.3, 1.7 Hz, 1H), 6.92–6.68 (m, 28H, Ar-CH), 5.11–5.01 (m, 1H, *N*-CH), 2.20–2.07 (m, 2H, CH_2), 1.80–1.66 (m, 2H, CH_2), 1.34 (s, 9H, CH_3), 1.33–1.30 (m, 27H, CH_3), 1.26–1.17 (m, 12H, CH_2), 1.13–1.08 (m, 27H, CH_3), 0.99 (s, 18H, CH_3), 0.84–0.77 ppm (m, 6H, CH_3). ^{13}C NMR (CD_2Cl_2, 126 MHz, 25 °C): δ = 165.0, 163.9 (C=O), 159.9, 156.6, 156.3, 156.2, 153.9, 153.9, 153.7, 153.6, 148.8, 148.5, 148.4, 148.0, 147.9, 147.8, 142.1, 141.4, 141.2, 141.0, 140.3, 139.9, 138.6, 138.5, 138.4, 134.2, 132.8, 131.8, 131.6, 131.5, 131.4, 130.5, 127.3, 127.22, 127.18, 124.0, 123.8, 123.7, 122.3, 121.7, 120.9, 120.2, 119.9, 119.8, 119.7, 119.3, 119.23, 119.15, 118.2, 116.1 (Ar-CH, Ar-C), 55.0 (*N*-CH), 34.87, 34.85, 34.84, 34.54, 34.52, 34.49, 32.9, 32.3, 31.80, 31.78, 31.5, 31.4, 27.1, 23.1, 14.4 ppm (CH_3, CH_2, C). MS (MALDI-TOF, dctb): m/z = 1947.6769 ($C_{137}H_{147}N_3O_7$ ([M]$^+$). HRMS: (MALDI-TOF, dctb): calculated for $C_{137}H_{147}N_3O_7$ ([M]$^+$) m/z = 1946.1234, found m/z = 1946.1226. UV/Vis (CH_2Cl_2): λ [nm] (ε [M^{-1} cm^{-1}]) = 451(12500), 573 (33500), 616 (49500). Fluorescence (CH_2Cl_2): $\lambda_{exc.}$ [nm] = 616, $\lambda_{emission}$ [nm] (rel. int.) = 654 (100).

Linear PDI–HPB (17): **17** was prepared according to GP II: Perylene-tolan **12** (20 mg, 15 μmol, 1 equiv.), tetracyclone **13** (9.0 mg, 15 μmol, 1 equiv.), toluene (0.5 mL); plug chromatography (SiO_2, DCM/hexanes 3:7); yield (blue solid) 84% (24 mg, 12 μmol). ^{1}H NMR (CD_2Cl_2, 400 MHz, 25 °C): δ = 8.31–8.24 (m, 2H, Ar-CH), 8.15–8.05 (m, 2H, Ar-CH), 7.93 (d, J = 8.2 Hz, 1H, Ar-CH), 7.35–7.24 (m, 9H, Ar-CH), 7.01 (dd, J = 8.4, 1.5 Hz, 1H, Ar-CH), 6.93–6.68 (m, 28H, Ar-CH), 5.08–5.01 (m, 1H, *N*-CH), 2.19–2.07 (m, 2H, CH_2), 1.77–1.69 (m, 2H, CH_2), 1.35 (s, 9H, CH_3), 1.32–1.29 (m, 27H, CH_3), 1.26–1.17 (m, 12H, CH_2), 1.13–1.07 (m, 27H, CH_3), 1.01 (s, 18H, CH_3), 0.83–0.78 ppm (m, 6H, CH_3). ^{13}C NMR (CD_2Cl_2, 126 MHz, 25 °C): δ = 165.0, 163.9 (C=O), 160.2, 156.6, 156.3, 153.9, 153.8, 153.6, 148.8, 148.5, 148.3, 148.0, 148.0, 147.9, 143.5, 141.23, 141.21, 141.0, 140.1, 140.0, 138.6, 138.5, 138.4, 134.2, 132.8, 131.7, 131.6, 131.52, 131.48, 130.2, 130.1, 127.3, 127.24, 127.22, 127.20, 123.9, 123.8, 123.71, 123.68, 123.3, 122.7, 121.6, 120.6, 120.2, 120.0, 119.9, 119.8, 119.2, 119.2, 116.3, 114.0 (Ar-CH, A-C), 55.0 (*N*-CH), 34.89, 34.85, 34.55, 34.52, 34.51, 32.9, 32.3, 31.82, 31.78, 31.5, 31.4, 27.1, 23.1, 14.4 ppm (CH_3, CH_2, C). MS (MALDI-TOF, dctb): m/z = 1947.3766 ($C_{137}H_{147}N_3O_7$ ([M]$^+$). HRMS: (APPI, ACN): calculated for $C_{137}H_{147}N_3O_7$ ([M]$^+$) m/z = 1946.1234, found m/z = 1946.1282. UV/Vis (CH_2Cl_2): λ [nm] (ε [M^{-1} cm^{-1}]) = 449 (14000), 567 (34500), 610 (52500). Fluorescence (CH_2Cl_2): $\lambda_{exc.}$ [nm] = 610, $\lambda_{emission}$ [nm] (rel. int.) = 646 (100).

Helical PDI–HBC (19): **19** was prepared according to GP III: PDI–HPB **15** (12 mg, 6.0 μmol, 1 equiv.), DCM (20 mL), dry $FeCl_3$ (16 mg, 98 μmol, 16 equiv.) $MeNO_2$ (0.06 mL); plug chromatography (SiO_2, DCM/hexanes 1:4); yield (blue/green solid) 95% (11 mg, 5.7 μmol). ^{1}H NMR ($C_2D_2Cl_4$, 500 MHz, 90 °C): δ = 9.74 (s, 1H, Ar-CH), 9.41 (s, 1H, Ar-CH), 9.36–9.25 (m, 7H, Ar-CH), 9.22 (s, 2H, Ar-CH), 8.75 (s, 1H, Ar-CH), 8.46 (s, 1H, Ar-CH), 8.34 (s, 1H, Ar-CH), 8.24–8.25 (m, 2H, Ar-CH), 7.38–7.15 (m, 8H, Ar-CH), 7.08–6.80 (m, 8H, Ar-CH), 5.07–5.00 (m, 1H, *N*-CH), 2.14–2.03 (m, 2H, CH_2), 1.85–1.75 (m, 38H, CH_2, CH_3), 1.53 (s, 9H, CH_3), 1.37 (s, 9H, CH_3), 1.34–1.30 (m, 18H, CH_3), 1.28 (s, 9H, CH_3), 1.27–1.18 (m, 12H, CH_2), 0.87–0.77 ppm (m, 6H, CH_2). ^{13}C NMR ($C_2D_2Cl_4$, 126 MHz, 90 °C): δ = 158.9 (C=O), 156.7, 156.4, 156.0, 154.0, 153.4, 153.3, 153.2, 152.3, 150.1, 150.0, 149.89, 149.87, 147.9, 147.73, 147.65, 147.6, 147.4, 145.5 (Ar-C), 134.0, 132.8, 131.1, 131.0, 130.92, 130.87, 130.80, 130.78, 130.76, 130.5, 129.3, 129.0, 127.2, 127.0, 126.9, 126.86, 126.85, 126.1, 126.0, 124.5, 124.3, 124.2, 124.0, 123.8, 122.4, 121.9, 121.7, 121.3, 121.1, 121.0, 120.8, 120.69, 120.66, 120.6, 120.2, 120.1, 120.0, 119.8, 119.62, 119.61, 119.55, 119.5, 119.4, 119.3, 119.1, 117.4, 113.8 (Ar-CH, Ar-C), 55.2 (*N*-CH), 36.0, 35.95, 35.94, 35.92, 35.7, 34.61, 34.56, 34.5, 32.8, 32.4, 32.28, 32.25, 32.23, 32.15, 32.1, 31.9, 31.8, 31.75, 31.73, 31.72, 26.9, 22.8, 22.7, 14.2, 14.1 ppm (CH_3, CH_2, C). MS (MALDI-TOF, dctb): m/z = 1935.0123 ($C_{137}H_{135}N_3O_7$ ([M]$^+$). HRMS: (APPI, CH_2Cl_2): calculated for $C_{137}H_{136}N_3O_7$ ([M+H]$^+$) m/z = 1935.0373, found m/z = 1935.0372. UV/Vis (CH_2Cl_2): λ [nm] (ε [M^{-1} cm^{-1}]) = 369 (73500), 600 (32000), 633 (35500).

Linear PDI–HBC (21): **21** was prepared according to GP III: PDI–HPB **17** (20 mg, 10 μmol, 1 equiv.), DCM (20 mL), dry $FeCl_3$ (27 mg,

0.16 mmol, 16 equiv.) $MeNO_2$ (0.1 mL); plug chromatography (SiO_2, DCM/hexanes 1:4); yield (blue/green solid) 85% (17 mg, 8.7 μmol). ^{1}H NMR ($C_2D_2Cl_4$, 500 MHz, 90 °C): δ = 11.58 (s, 1H, Ar-CH), 10.41 (s, 1H, Ar-CH), 9.39 (s, 1H, Ar-CH), 9.35–9.18 (m, 8H, Ar-CH), 9.00 (s, 1H, Ar-CH), 8.64 (s, 1H, Ar-CH), 8.23 (s, 1H, Ar-CH), 8.16 (s, 1H, Ar-CH), 7.37–7.30 (m, 4H, Ar-CH), 7.28–7.22 (m, 4H, Ar-CH), 7.15–7.09 (m, 2H, Ar-CH), 7.00–6.96 (m, 2H, Ar-CH), 6.93–6.88 (m, 2H, Ar-CH), 6.82–6.77 (m, 2H, Ar-CH), 5.07–4.99 (m, 1H, *N*-CH), 2.15–2.03 (m, 2H, CH_2), 1.84–1.77 (m, 38H, CH_3, CH_2), 1.61 (s, 9H, CH_3), 1.38 (s, 9H, CH_3), 1.36 (s, 9H, CH_3), 1.32 (s, 9H, CH_3), 1.31 (s, 9H, CH_3), 1.28–1.21 (m, 12H, CH_2), 0.85–0.79 ppm (m, 6H, CH_3). ^{13}C NMR ($C_2D_2Cl_4$, 126 MHz, 90 °C): δ = 160.7 (C=O), 156.6, 156.5, 156.1, 156.0, 154.5, 153.7, 153.3, 153.1, 150.3, 150.0, 149.9, 149.8, 149.7, 148.7, 147.8, 147.7, 147.1, 140.9, 134.2, 132.5, 132.4, 131.2, 131.02, 130.98, 130.93, 130.87, 130.85, 130.7, 130.2, 130.1, 129.9, 127.0, 126.97, 126.87, 125.4, 124.4, 124.22, 124.15, 124.1, 124.0, 123.8, 123.2, 122.7, 121.8, 121.3, 121.10, 121.09, 121.0, 120.9, 120.8, 120.63, 120.57, 120.5, 120.4, 120.2, 120.0, 119.9, 119.8, 119.6, 119.5, 119.41, 119.36, 119.30, 119.29, 119.12, 119.11, 118.8, 117.9, 109.2 (Ar-CH; Ar-C), 55.2 (*N*-CH), 36.1, 36.0, 35.92, 35.90, 34.6, 34.59, 34.58, 34.56, 32.8, 32.4, 32.3, 32.2, 32.0, 31.9, 31.8, 31.75, 31.74, 26.9, 22.7, 14.2 ppm (CH_3, CH_2, C). MS (MALDI-TOF, dctb): m/z = 1935.4253 ($C_{137}H_{135}N_3O_7$ ($[M]^+$). HRMS: (MALDI-TOF, dctb): calculated for $C_{137}H_{135}N_3O_7$ ($[M]^+$) m/z = 1934.0295, found m/z = 1934.0266. UV/Vis (CH_2Cl_2): λ [nm] (ε [M^{-1} cm^{-1}]) = 369 (81000), 628 (35000), 663 (32000).

Acknowledgements

The authors thank the Deutsche Forschungsgemeinschaft (DFG—SFB 953 "Synthetic Carbon Allotropes", and the Graduate School Molecular Science (GSMS) for financial support. Open access funding enabled and organized by Projekt DEAL.

Conflict of interest

The authors declare no conflict of interest.

Keywords: charge transfer · helicene · hexabenzocoronene HBC · rylenediimide · transient absorption

[1] a) F. Cacialli, J. S. Wilson, J. J. Michels, C. Daniel, C. Silva, R. H. Friend, N. Severin, P. Samorì, J. P. Rabe, M. J. O'Connell, P. N. Taylor, H. L. Anderson, *Nat. Mater.* **2002**, *1*, 160–164; b) F. Cacialli, P. Samorì, C. Silva, *Mater. Today* **2004**, *7*, 24–32; c) H. Sirringhaus, *Adv. Mater.* **2005**, *17*, 2411–2425; d) W. Pisula, A. Menon, M. Stepputat, I. Lieberwirth, U. Kolb, A. Tracz, H. Sirringhaus, T. Pakula, K. Müllen, *Adv. Mater.* **2005**, *17*, 684–689; e) A. Facchetti, *Mater. Today* **2007**, *10*, 28–37; f) A. R. Murphy, J. M. J. Fréchet, *Chem. Rev.* **2007**, *107*, 1066–1096; g) V. Coropceanu, J. Cornil, D. A. da Silva Filho, Y. Olivier, R. Silbey, J.-L. Brédas, *Chem. Rev.* **2007**, *107*, 926–952; h) B. A. Jones, A. Facchetti, M. R. Wasielewski, T. J. Marks, *Adv. Funct. Mater.* **2008**, *18*, 1329–1339; i) M. Mas-Torrent, C. Rovira, *Chem. Soc. rev.* **2008**, *37*, 827–838; j) F. J. M. Hoeben, P. Jonkheijm, E. W. Meijer, A. P. H. J. Schenning, *Chem. Rev.* **2005**, *105*, 1491–1546.

[2] a) A. Fechtenkötter, K. Saalwächter, M. A. Harbison, K. Müllen, H. W. Spiess, *Angew. Chem. Int. Ed.* **1999**, *38*, 3039–3042; *Angew. Chem.* **1999**, *111*, 3224–3228; b) D. Käfer, A. Bashir, X. Dou, G. Witte, K. Müllen, C. Wöll, *Adv. Mater.* **2010**, *22*, 384–388; c) J. Wu, M. D. Watson, N. Tchebotareva, Z. Wang, K. Müllen, *J. Org. Chem.* **2004**, *69*, 8194–8204; d) J. Wu, W. Pisula, K. Müllen, *Chem. Rev.* **2007**, *107*, 718–747; e) K. Müllen, J. P. Rabe, *Acc. Chem. Res.* **2008**, *41*, 511–520; f) A. M. van de Craats, J. M. Warman, A. Fechtenkötter, J. D. Brand, M. A. Harbison, K. Müllen, *Adv. Mater.* **1999**, *11*, 1469–1472; g) P. Haines, D. Reger, J. Träg, V. Strauss, D. Lungerich, D. Zahn, N. Jux, D. Guldi, *Nanoscale* **2021**, *13*, 801–809.

[3] a) F. Würthner, *Chem. Commun.* **2004**, 1564–1579; b) C. W. Struijk, A. B. Sieval, J. E. J. Dakhorst, M. van Dijk, P. Kimkes, R. B. M. Koehorst, H. Donker, T. J. Schaafsma, S. J. Picken, A. M. van de Craats, J. M. Warman, H. Zuilhof, E. J. R. Sudhölter, *J. Am. Chem. Soc.* **2000**, *122*, 11057–11066; c) Z. Chen, M. G. Debije, T. Debaerdemaeker, P. Osswald, F. Würthner, *ChemPhysChem* **2004**, *5*, 137–140; d) T. Weil, T. Vosch, J. Hofkens, K. Peneva, K. Müllen, *Angew. Chem. Int. Ed.* **2010**, *49*, 9068–9093; *Angew. Chem.* **2010**, *122*, 9252–9278; e) C. Jung, B. K. Müller, D. C. Lamb, F. Nolde, K. Müllen, C. Bräuchle, *J. Am. Chem. Soc.* **2006**, *128*, 5283–5291.

[4] a) C. Im, W. Tian, H. Bässler, A. Fechtenkötter, M. D. Watson, K. Müllen, *J. Chem. Phys.* **2003**, *119*, 3952–3957; b) H. C. Hesse, J. Weickert, M. Al-Hussein, L. Dössel, X. Feng, K. Müllen, L. Schmidt-Mende, *Sol. Energy Mater. Sol. Cells* **2010**, *94*, 560–567; c) L. Schmidt-Mende, A. Fechtenkötter, K. Müllen, E. Moons, R. H. Friend, J. D. MacKenzie, *Science* **2001**, *293*, 1119–1122; d) J. L. Li, M. Kastler, W. Pisula, J. W. F. Robertson, D. Wasserfallen, A. C. Grimsdale, J. S. Wu, K. Müllen, *Adv. Funct. Mater.* **2007**, *17*, 2528–2533; e) M. Al-Hussein, H. C. Hesse, J. Weickert, L. Dössel, X. Feng, K. Müllen, L. Schmidt-Mende, *Thin Solid Films* **2011**, *520*, 307–313; f) G. de Luca, A. Liscio, M. Melucci, T. Schnitzler, W. Pisula, C. G. Clark, L. M. Scolaro, V. Palermo, K. Müllen, P. Samorì, *J. Mater. Chem.* **2010**, *20*, 71–82; g) J. Jung, A. Rybak, A. Slazak, S. Bialecki, P. Miskiewicz, I. Glowacki, J. Ulanski, S. Rosselli, A. Yasuda, G. Nelles, Ž. Tomović, M. D. Watson, K. Müllen, *Synth. Met.* **2005**, *155*, 150–156; h) J. Piris, M. P. de Haas, J. M. Warman, K. Müllen, A. Fechtenkötter, A. M. van de Craats, L. Schmidt-Mende, R. H. Friend, *Synth. Met.* **2003**, *137*, 1375–1376; i) C. Im, W. Tian, H. Bässler, A. Fechtenkötter, M. D. Watson, K. Müllen, *Synth. Met.* **2003**, *139*, 683–686.

[5] a) W.-S. Li, Y. Yamamoto, T. Fukushima, A. Saeki, S. Seki, S. Tagawa, H. Masunaga, S. Sasaki, M. Takata, T. Aida, *J. Am. Chem. Soc.* **2008**, *130*, 8886–8887; b) N. Tchebotareva, X. Yin, M. D. Watson, P. Samorì, J. P. Rabe, K. Müllen, *J. Am. Chem. Soc.* **2003**, *125*, 9734–9739; c) P. Samori, X. Yin, N. Tchebotareva, Z. Wang, T. Pakula, F. Jäckel, M. D. Watson, A. Venturini, K. Müllen, J. P. Rabe, *J. Am. Chem. Soc.* **2004**, *126*, 3567–3575; d) C. Röger, M. G. Müller, M. Lysetska, Y. Miloslavina, A. R. Holzwarth, F. Würthner, *J. Am. Chem. Soc.* **2006**, *128*, 6542–6543; e) Y. Yamamoto, T. Fukushima, Y. Suna, N. Ishii, A. Saeki, S. Seki, S. Tagawa, M. Taniguchi, T. Kawai, T. Aida, *Science* **2006**, *314*, 1761–1764; f) N. S. Sariciftci, L. Smilowitz, A. J. Heeger, F. Wudl, *Science* **1992**, *258*, 1474–1476.

[6] a) M. R. Wasielewski, M. P. Niemczyk, *J. Am. Chem. Soc.* **1984**, *106*, 5043–5045; b) N. S. Sariciftci, A. Werner, A. Grupp, M. Mehring, G. Götz, P. Bäuerle, F. Effenberger, *Mol. Phys.* **1992**, *75*, 1259–1267.

[7] a) L. F. Dössel, V. Kamm, I. A. Howard, F. Laquai, W. Pisula, X. Feng, C. Li, M. Takase, T. Kudernac, S. de Feyter, K. Müllen, *J. Am. Chem. Soc.* **2012**, *134*, 5876–5886; b) S. Wang, L. Dössel, A. Mavrinskiy, P. Gao, X. Feng, W. Pisula, K. Müllen, *Small* **2011**, *7*, 2841–2846; c) J. M. Mativetsky, M. Kastler, R. C. Savage, D. Gentilini, M. Palma, W. Pisula, K. Müllen, P. Samorì, *Adv. Funct. Mater.* **2009**, *19*, 2486–2494; d) J. Wu, J. Qu, N. Tchebotareva, K. Müllen, *Tetrahedron Lett.* **2005**, *46*, 1565–1568; e) P. Samorì, A. Fechtenkötter, E. Reuther, M. D. Watson, N. Severin, K. Müllen, J. P. Rabe, *Adv. Mater.* **2006**, *18*, 1317–1321.

[8] a) C. Dusold, B. Platzer, P. Haines, D. Reger, N. Jux, D. Guldi, A. Hirsch, *Chem. Eur. J.* **2021**, *27*, 1670–1679; b) M. M. Martin, C. Dusold, A. Hirsch, N. Jux, *J. Porphyrins Phthalocyanines* **2020**, *24*, 268–277.

[9] C. Dusold, D. I. Sharapa, F. Hampel, A. Hirsch, *Chem. Eur. J.* **2021**, *27*, 2332–2341.

[10] Y. Lin, Q. Song, *Eur. J. Org. Chem.* **2016**, 3056–3059.

[11] a) M. M. Martin, D. Lungerich, P. Haines, F. Hampel, N. Jux, *Angew. Chem. Int. Ed.* **2019**, *58*, 8932–8937; *Angew. Chem.* **2019**, *131*, 9027–9032; b) D. Reger, P. Haines, F. W. Heinemann, D. M. Guldi, N. Jux, *Angew. Chem. Int. Ed.* **2018**, *57*, 5938–5942; *Angew. Chem.* **2018**, *130*, 6044–6049.

[12] B. S. Basel, J. Zirzlmeier, C. Hetzer, S. R. Reddy, B. T. Phelan, M. D. Krzyaniak, M. K. Volland, P. B. Coto, R. M. Young, T. Clark, M. Thoss, R. R. Tykwinski, M. R. Wasielewski, D. M. Guldi, *Chem* **2018**, *4*, 1092–1111.

Manuscript received: December 7, 2020
Accepted manuscript online: January 25, 2021
Version of record online: March 10, 2021

